Supporting Information

# Hierarchical Porous Dual-mode Thermal Management Fabrics Achieved by Regulating Solar and Body Radiations

Chuntao Lan[a], Jia Meng[a], Chongxiang Pan[a], Luyao Jia[a, b], Xiong Pu[a, b, *]

[a] CAS Center for Excellent in Nanoscience, Beijing Key Laboratory of Micro-nano Energy and Sensor, Beijing Institute of Nanoenergy and Nanosystems, Chinese Academy of Sciences, Beijing 101400, China.

[b] School of Nanoscience and Engineering, University of Chinese Academy of Sciences, Beijing 100049, China.

*Corresponding author. E-mail: puxiong@binn.cas.cn

**Supplementary Note**

**Experimental Section**

*Materials*: Polyacrylonitrile (PAN, $M_W$=85000), Lithium fluoride (LiF, 99.99% metal basis) and *N,N*-Dimethylformamide (DMF) were purchased from Macklin (Shanghai, China). Poly(vinylpyrrolidone) (PVP, $M_W$=1300000) was bought from Aladdin. Ternary carbide ($Ti_3AlC_2$) MAX phase powder was obtained from 11 Technology Co., Ltd. (Jilin, China). Concentrated hydrochloric acid (HCl) was provided by Sinopharm Chemical Reagent Co., Ltd. All chemicals were used as received without any further purification.

*Preparation of PPAN fabric*: PAN/PVP fabric was firstly formed by the electrospinning technique.[1] Briefly, 8 wt% PAN powder and corresponding PVP powder were slowly added into DMF. The blended solution was stirred overnight. The PAN/PVP weight ratios were set to be 1:1 and 1:2, separately. Without further statement, the weight ratio of PAN/PVP fabric used in this work was 1:2. Then, the PAN/PVP fabrics were prepared by an electrospinning machine. For the electrospinning procedure, the tip-to-collector distance was 20 cm, the voltage was 22 kV, and the feed rate of PAN/PVP solution was set to be 1.5 mL/h. The composite fabric was collected on an aluminum foil through a rotating roller. The speed of the roller was 300 rpm. The duration of the electrospinning process was set to be 4 h, 6 h, 8 h to acquire fabrics with different thicknesses. Without further statement, PAN/PVP fabric used in this work was obtained after 6-h electrospinning. After that, a free-standing PAN/PVP fabric was peeled off from the foil. The as-prepared PAN/PVP fabric was then placed in a Teflon-lined stainless-steel autoclave with an appropriate amount of Deionized water. The device was heated at 100 ℃ for 10 h to selectively remove PVP through the phase separation. After that, the fabric was washed with plenty water to thoroughly remove the residual PVP. Finally, PPAN fabric with hierarchical pores was obtained after drying the sample in an oven at 60 ℃ for 1 h.

*Fabrication of Janus fabric*: The as-prepared PPAN was acted as the substrate for Janus fabric. For MXene/PPAN, MXene suspension was synthesized through a wet-etching method which has been reported previously.[2] MXene layer decorated on one

side of PPAN fabric through a scalable brush-coating method with (20 mg/mL) MXene suspension and dried at 60 ℃. MXene coating mass on PPAN was 0.25 mg/cm$^2$. For metallic Janus fabrics (i.e., Ag, Cu, Ni), they were prepared through the magnetron sputtering system (Denton Discovery635) equipped with Ag, Cu, Ni target, respectively. The deposition time was 20 min under constant sputtering power of 30 W and flow velocity of argon gas of 30 sccm.

*Outdoor thermal measurement*: As schematically demonstrated in Figure 3b, a homemade device was used for outdoor thermal measurements of fabrics. The box was mainly composed of polystyrene foam for thermal insulation with an opening side. The outside of the foam box was wrapped with a layer of aluminum foil to reflect the heat from surroundings. A silicon rubber heating plate was utilized to simulate the skin and situated inside the box. The fabric was placed above the simulated skin with a *T*-type thermocouple between them to record the temperature of the skin. Another thermocouple is putted in the box and far away from the heating plate to record the ambient temperature. A layer of polyethylene film covers the top of the foam box to avoid the influence of wind. The tests were performed on the roof of a building in Huai Rou, Beijing, China (40°24’14’’ N, 116°40’32’’ E,) under sunlight irradiation in August, 2022. The solar irradiance during the tests was recorded through a pyranometer.

*Characterizations*: The micro morphologies of fabrics were obtained by a field emission scanning electron microscope (FESEM, Hitachi SU8020) operating at 5 kV. The porous structure of PPAN fibers was further observed through a transmission electron microscope (TEM, FEI Tecnai G2F20 S-TWIN TMP). The pore size distribution of PPAN was measured by an automatic mercury porosimeter (Micrometritics AutoPore V 9620) and an automatic surface and porosity analyzer BET (Quantachrome Autosorb IQ). The infrared absorption spectra of fabrics were measured by a Fourier transformed infrared (FTIR) spectrometer (Bruker VERTEX80v). The ultraviolet-visible-near-infrared spectroscopy of fabrics was achieved by an ultraviolet spectrophotometer (Shimadzu UV3600) with a barium sulphate integrating sphere. The reflectance and transmittance were recorded by an FTIR spectrometer (Nicolet iS50)

with a gold diffuse integrating sphere. The IR thermal image was taken by an IR thermometer (FOTRIC 226-2). The mechanical tensile stress of fabrics was measured through a universal testing machine (Yuelian SAS-50KG). Air permeability tests were conducted using YG461E-III (Wuhan Guoliang Instrument Co. Ltd.) according to ASTM D737-2018. The UV ageing of PPAN was conducted in a Xenon Weather-Ometer (Atlas CI4000) according to ISO4892-2.

**Note S1. Finite-Difference-Time-Domain Simulations**

To unveil the significant role of the hierarchical porous structure in PPAN fabric, Finite-Difference-Time-Domain (FDTD) simulations were carried out using Lumerical FDTD Solution software. Due to computational constraints of the computer, two dimensional (2D) models with the size of 5×30 $\mu m^2$ were firstly used for the calculation of reflectance (Figure 3e). To simplify the structure of fabric, PAN film with hierarchical pores was built where the diameter of micropores was set to be 1.3 μm and that of nanopores was 10-100 nm and in accordance with normal distribution. The porosity of the film was 0.66. The ratio of micropores to nanopores was 94:6. The pores were randomly distributed in the film. Then, the models of PAN film with one micropore (Figure 3d<i>) and one micropore with several nanopores (Figure 3d<ii>) were conducted to demonstrate the significant role of nanopores. The size of models was 4.2×4.2 $\mu m^2$.

Periodic boundary was used along the x-axis and the perfect match layer (PML) boundary was used along the y-axis to absorb the scattering waves. Transverse electric (TE) and transverse magnetic (TM) polarized plane wave was used as the light source and the injection light wavelength was from 400 to 900 nm. A monitor was placed above the incident plane to monitor the reflectance. The reflectance results were calculated by averaging the results for TE and TM polarizations.

**Note S2. The photothermal conversion efficiency of MXene/PPAN fabric**

The photothermal conversion efficiencies of MXene/PPAN fabric was calculated based on the following equation:

$$\eta = \frac{I_{fabric}}{I_{solar}} = \frac{Cm\Delta T}{P_{solar}St} x100\% \quad \text{S1}$$

where $I_{fabric}$ is the heat generated by the light on the surface of the film. $I_{solar}$ is the heat of the sunlight reaching the surface of the film. $C$ is the specific heat capacity of the fabric, which is measured using a differential scanning calorimeter (STA 449F3). $m$ is the weight of the fabric. $\Delta T$ is the change in fabric temperature values. $P_{solar}$ is the power of the solar irradiation at the surface of the fabric. $S$ is the illuminated area of the fabric surface. $t$ is the exposure time under sunlight. The $\eta$ of MXene/PPAN was calculated to be 37.5%.

**Note S3. The set-point after covered with the Janus fabric**

In an indoor environment, we could assume people generate and dissipate heat steadily. The heat flux transfer between human skin and ambient could be described as the following equation:

$$q_{skin} = h_{eff}(T_{skin,0} - T_{amb}) \quad \text{S2}$$

Here, $q_{skin}$ is the heat flux of skin, which is ~100 W/m$^2$; $h_{eff}$ is the effective thermal transfer coefficient, considering thermal transfer via conduction, convection and radiation. $T_{skin,0}$ and $T_{amb}$ are skin temperature and ambient temperature. In the simulated skin temperature test, $q_{skin}$ (34.2 ℃) and $T_{amb}$ (25 ℃) are the same. $T_{skin,0}$ has been recorded after covered with the Janus fabric in heating (39.5 ℃) or in cooling mode (34.5 ℃) in our experiment. Then, $h_{eff}$ could be calculated.

For personal thermal comfort, we assume human skin temperature is kept at 34.2 ℃. Therefore, $T_{amb}$, that is set-point ($T_{set\text{-}point}$), has to be changed to satisfy the above equation. To calculate the set point of building ($T_{set\text{-}point}$), the above equation could be converted into:

$$T_{amb} = T_{set-point} = T_{skin,1} - \frac{q_{skin}}{h_{eff}} \quad \text{S3}$$

Here, $T_{skin,1}$=34.2 ℃. $\frac{q_{skin}}{h_{eff}} = T_{skin,0} - T_{amb}$. Therefore, the set-point with the fabric in

the heating mode is calculated to be $T_{set\text{-}point}$=34.2 ℃–($T_{skin,0}$–$T_{amb}$)=19.7 ℃. At the expanded heating setpoint from 25 ℃ to 19.7 ℃, the energy savings is more than 30%.[3]

**Table S1.** Brand, item number and content of the sun-protective clothing used for the temperature test in Figure S5c.

| Number | Brand | Item. No | Fabric content |
|---|---|---|---|
| #1 | Jeanswest | ZWSFSY22040903 | 90% polyester, 10% spandex |
| #2 | Camel | A012252009 | 100% polyester |
| #3 | Xtep | 878228140418 | 86% nylon, 14% spandex |

**Table S2.** Comparison of PTM fabrics and their cooling/heating performances reported in literature and in this work. MXene/PTM stands itself out both outdoor and indoor conditions from many other thermoregulation fabrics.

| Materials | Mode | Ref. |
|---|---|---|
| MXene/PPAN | Outdoor cooling (14 ℃), outdoor heating (4 ℃), indoor heating (5.3 ℃), indoor cooling (0.3 ℃) | This work |
| TPU membrane | Outdoor cooling (10 ℃), outdoor heating (9.5 ℃) | [4] |
| PMMA/ePTFE/Al/nanoPE/Zn-CuNPs | Outdoor cooling (6 ℃), outdoor heating (8.1 ℃) | [5] |
| PPy/PVDF-HFP | Outdoor cooling (3 ℃), outdoor heating (10 ℃) | [6] |
| ZnO/PE nanofabric | Outdoor cooling (11 ℃) | [7] |
| Cellulose aerogel membrane/ZnO-TPU | Outdoor cooling (9.3 ℃) | [8] |

| | | |
|---|---|---|
| ZIF-8-TPU | Outdoor Cooling (7.2 ℃) | [9] |
| PVDF nanofabric | Outdoor cooling (12 ℃) | [10] |
| $P(VdF\text{-}HFP)_{HP}$ coated cotton fabric | Outdoor cooling (10 ℃) | [11] |
| PDMS/PTW@cotton fabric | Outdoor cooling (4.2 ℃) | [12] |
| Cellulose acetate/cotton/fluoropolymer | Outdoor cooling (4.2 ℃) | [13] |
| PA/PVDF/PE fabric | Outdoor cooling (4.5 ℃) | [14] |
| PTFE/$TiO_2$-PLA fabric | Outdoor cooling (10.2 ℃) | [15] |
| $Al_2O_3$-CA/$SiO_2$-PA6 fabric | Outdoor cooling (8 ℃) | [16] |
| Au-Ge/nanoPE | Outdoor heating (6.3 ℃), indoor heating (3.8 ℃) | [17] |
| NanoPE fabric | Indoor cooling (1.3 ℃) | [18] |
| Bilayer nanoPE fabric | Indoor cooling (1 ℃) | [19] |
| $Si_3N_4$@PVDF/nanoPE fabric | Indoor cooling (0.2 ℃) | [20] |
| MXene/nanoPE | Indoor heating (6.2 ℃) | [21] |
| AgNWs/cotton fabric | Indoor heating (0.9 ℃) | [22] |

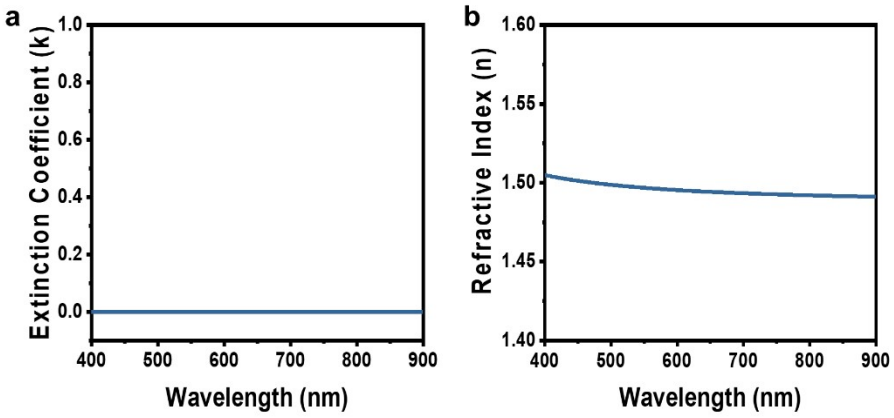


**Figure S1.** (a) extinction coefficient and (b) refractive index of pure PAN film. The high refractive index and low extinction coefficient indicates this material with highly porous structure is suitable for passive daytime radiative cooling.

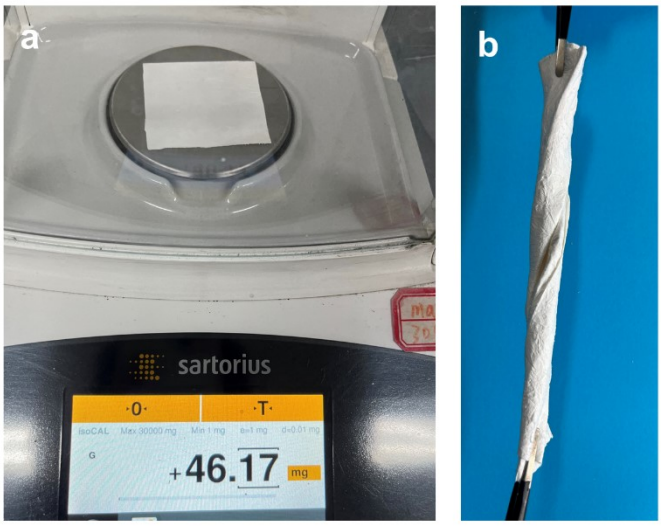


**Figure S2.** Optical images of (a) the weight of one piece of PPAN with a dimension of 5×5 $cm^2$, (b) the twisted PPAN fabric. These photographs show the light weight and flexibility of PPAN fabric.

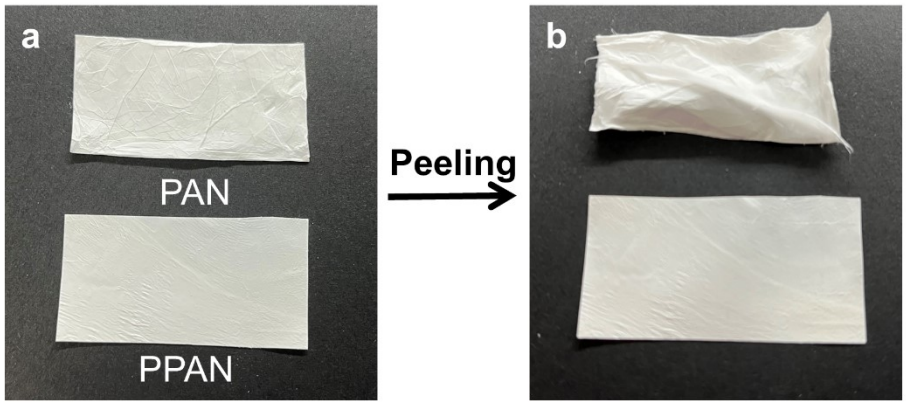


**Figure S3.** Photo images of PAN and PPAN fabrics (a) before and (b) after one adhesive-peeling cycle, exhibiting the mechanical stability of PPAN.

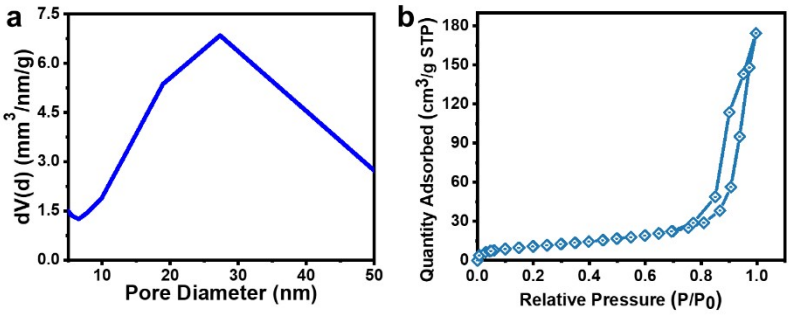


**Figure S4.** (a) the pore size distribution of PPAN among meso-level. (b) $N_2$ adsorption-desorption isotherm of PPAN.

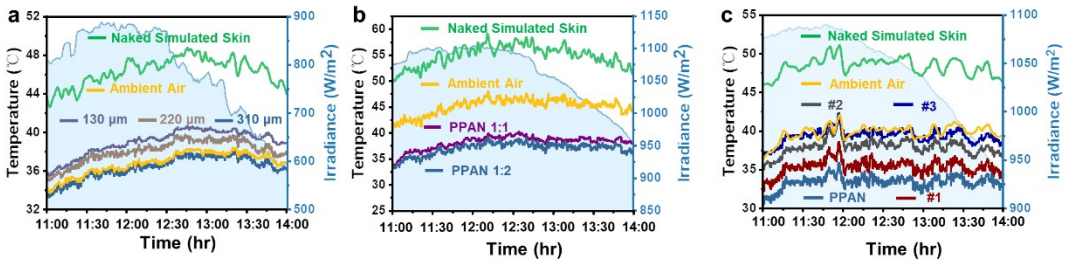


**Figure S5.** The real-time temperature of the simulated skin after covered with (a) PPAN with different thicknesses, (b) different masses of sacrificial template. (c) The comparison of the real-time temperature of simulation skin with PPAN and three different brands of commercial sun-protective clothing.

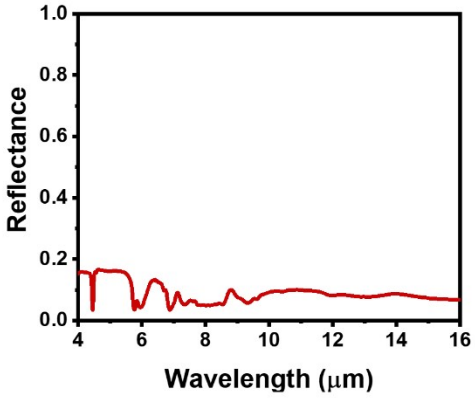


**Figure S6.** Spectral reflectance of PPAN in the 4-16 μm wavelength range.

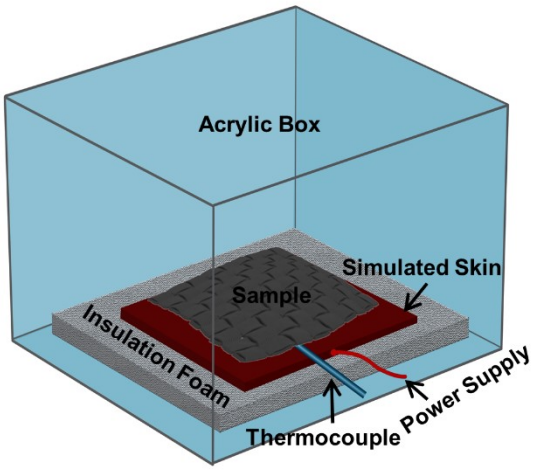


**Figure S7.** Schematic representation of the thermal measurement setup for indoor environment. The heating plate was equipped with automatic voltage regulator. The variation of the heating plate was set to be ±0.5 ℃.

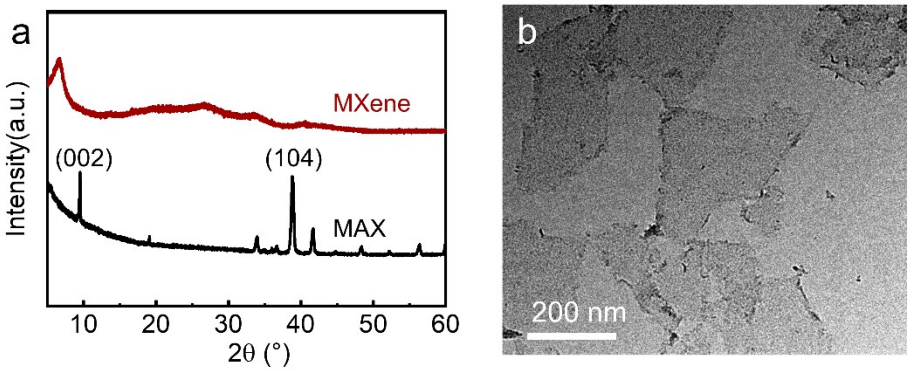


**Figure S8.** (a) XRD patterns of MXene and MAX phase. The disappearance of the (104) peak of the MAX and the shift of the (002) peak in the XRD pattern confirm the elimination of Al after the acid etching and the expansion of the sheets' spacing at the same time. (b) TEM image of MXene sheets. The as-obtained MXene exhibits a typical sheet-like morphology with a lateral size of hundreds of nanometers.

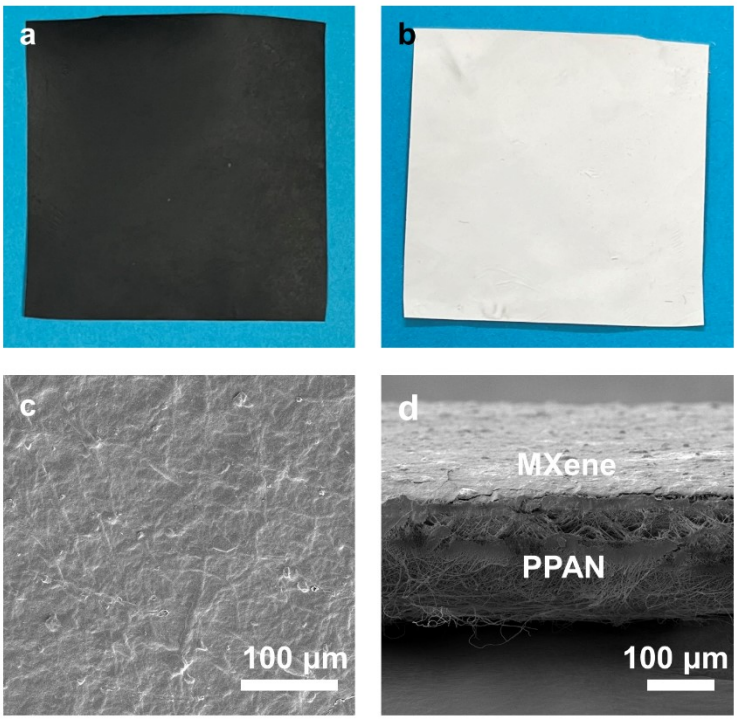


**Figure S9.** Photo images of (a) MXene/PPAN F, (b) MXene/PPAN R, exhibiting the Janus structure of the fabric. SEM images of (c) MXene/PPAN F, (d) cross section of the Janus fabric.


**Figure S10.** Photograph of MXene/PPAN R (left) and MXene/PPAN F(right) integrated with a coat.

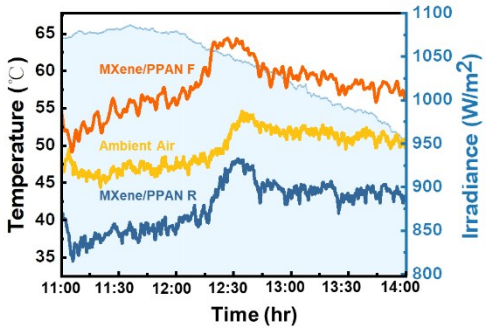


**Figure S11.** The real-time temperature of the ambient and the foam covered with MXene/PPAN F, MXene/PPAN R under sunlight irradiation outside.

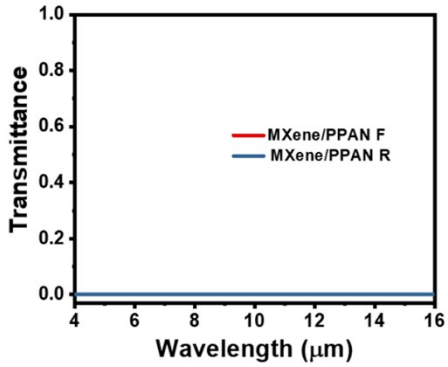


**Figure S12.** Spectral transmittance of MXene/PPAN F and MXene/PPAN R.

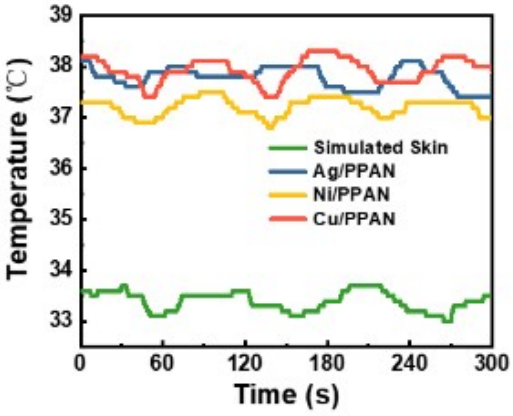


**Figure S13.** The real-time temperature of the simulated skin with Ag/PPAN, Ni/PPAN, Cu/PPAN cover and without cover.

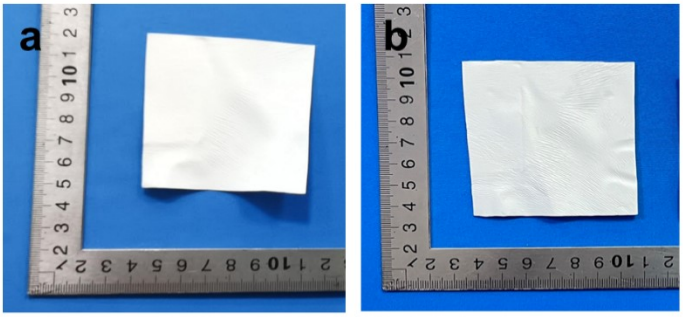


**Figure S14.** Photo images of PPAN (a) before and (b) after 100-h UV irradiation.

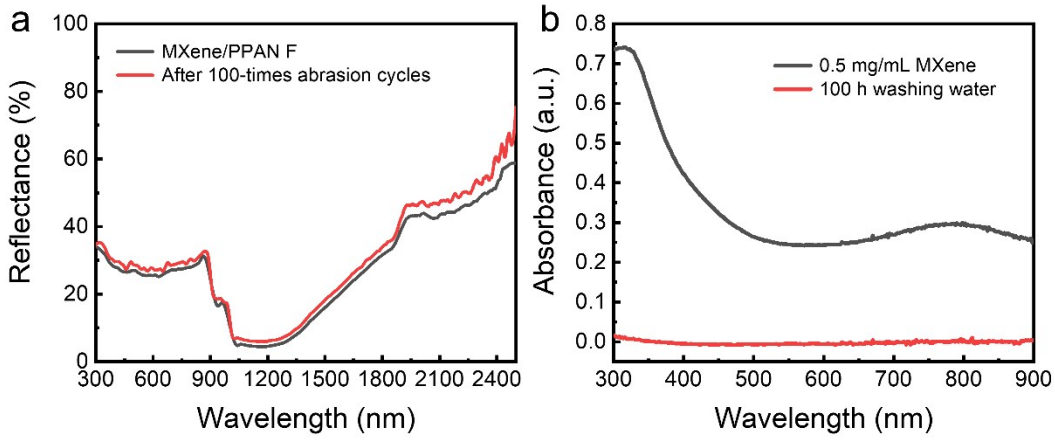


**Figure S15.** (a) The reflectance spectra of MXene/PPAN F before and after 100-times abrasion cycles. For the abrasion-resistant test, MXene/PPAN F was scratched repeatedly with a piece of 800-mesh sandpaper under a 100 g mass. Reflectance spectra of MXene/PPAN F before and after 100-times scratch were measured. (b) The absorbance spectrum of the 100-h washing water of Janus fabrics. As a reference, 0.5 mg/mL MXene suspension was measured. The washing stability of the Janus fabric was conducted according to a modified ISO 105-C10:2006 where the fabric was placed in a homemade machine at a spinning rate of 40 rpm and 40 °C with a liquor ratio of 10:1.

**References:**

[1] Zhang Y, Guan J, Wang X, Yu J, Ding B. Balsam-Pear-Skin-Like Porous Polyacrylonitrile Nanofibrous Membranes Grafted with Polyethyleneimine for Postcombustion CO2 Capture. *ACS Appl. Mater. Interfaces* **2017**, *9* (46), 41087-41098.

[2] Lan C, Jia H, Qiu M, Fu S. Ultrathin MXene/Polymer Coatings with an Alternating

Structure on Fabrics for Enhanced Electromagnetic Interference Shielding and Fire-Resistant Protective Performances. *ACS Appl Mater Interfaces* **2021**, *13* (32), 38761-38772.

[3] KHL TH, Zhang H, Arens E, Webster T. Energy Savings from Extended Air Temperature Setpoints and Reductions in Room Air Mixing. *International Conference on Environmental Ergonomics* **2009**, *August 2-7, Boston*.

[4] Li X, Ding Z, Lio GE, Zhao J, Xu H, Pattelli L, Pan L, Li Y. Strain-Adjustable Reflectivity of Polyurethane Nanofiber Membrane for Thermal Management Applications. *Chem. Eng. J.* **2023**, *461*, 142095.

[5] Luo H, Zhu Y, Xu Z, Hong Y, Ghosh P, Kaur S, Wu M, Yang C, Qiu M, Li Q. Outdoor Personal Thermal Management with Simultaneous Electricity Generation. *Nano Lett* **2021**, *21* (9), 3879-3886.

[6] Xiang B, Zhang R, Zeng X, Luo Y, Luo Z. An Easy-to-Prepare Flexible Dual-Mode Fiber Membrane for Daytime Outdoor Thermal Management. *Adv. Fiber Mater.* **2022**, *4* (5), 1058-1068.

[7] Iqbal MI, Lin K, Sun F, Chen S, Pan A, Lee HH, Kan CW, Lin CSK, Tso CY. Radiative Cooling Nanofabric for Personal Thermal Management. *ACS Appl. Mater. Interfaces* **2022**, *14*, 23577-23587.

[8] Gu B, Fan F, Xu Q, Shou D, Zhao D. A Nano-structured Bilayer Asymmetric Wettability Textile for Efficient Personal Thermal and Moisture Management in High-temperature Environments. *Chem. Eng. J.* **2023**, *461*, 141919.

[9] Cai X, Gao L, Wang J, Li D. MOF-Integrated Hierarchical Composite Fiber for Efficient Daytime Radiative Cooling and Antibacterial Protective Textiles. *ACS Appl. Mater. Interfaces* **2023**, *15* (6), 8537-8545.

[10] Kim G, Park K, Hwang KJ, Jin S. Highly Sunlight Reflective and Infrared Semi-Transparent Nanomesh Textiles. *ACS Nano* **2021**, *15* (10), 15962-15971.

[11] Sun Y, Ji Y, Javed M, Li X, Fan Z, Wang Y, Cai Z, Xu B. Preparation of Passive Daytime Cooling Fabric with the Synergistic Effect of Radiative Cooling and Evaporative Cooling. *Adv. Mater. Technol.* **2021**, *7* (3).

[12] Ni Y, Shen G, Ng KH, Zhu T, Li S, Li X, Cai W, Chen Z, Huang J. Rational

Construction of Superhydrophobic PDMS/PTW@cotton Fabric for Efficient UV/NIR Light Shielding. *Cellulose* **2022**, *29* (8), 4673-4685.

[13] Miao D, Cheng N, Wang X, Yu J, Ding B. Sandwich-structured Textiles with Hierarchically Nanofibrous Network and Janus Wettability for Outdoor Personal Thermal and Moisture Management. *Chem. Eng. J.* **2022**, *450*, 138012.

[14] Song YN, Li Y, Yan DX, Lei J, Li ZM. Novel Passive Cooling Composite Textile for Both Outdoor and Indoor Personal Thermal Management. *Compos. Part A-Appl. S.* **2020**, *130*, 105738.

[15] Zeng S, Pian SP, Su M, Wang Z, Wu M, Liu X, Chen M, Xiang Y, Wu J, Zhang M, Cen Q, Tang Y, Zhou X, Huang Z, Wang R, Tunuhe A, Sun X, Xia Z, Tian M, Chen M, Ma X, Yang L, Zhou J, Zhou H, Yang Q, Li X, Ma Y, Tao G. Hierarchical-Morphology Metafabric for Scalable Passive Daytime Radiative Cooling. *Science* **2021**, *33*, 692-696.

[16] Zhang X, Yang W, Shao Z, Li Y, Su Y, Zhang Q, Hou C, Wang H. A Moisture-Wicking Passive Radiative Cooling Hierarchical Metafabric. *ACS Nano* **2022**, *16* (2), 2188-2197.

[17] Luo H, Li Q, Du K, Xu Z, Zhu H, Liu D, Cai L, Ghosh P, Qiu M. An Ultra-thin Colored Textile with Simultaneous Solar and Passive Heating Abilities. *Nano Energy* **2019**, *65*, 103998.

[18] Peng Y, Chen J, Song AY, Catrysse PB, Hsu P-C, Cai L, Liu B, Zhu Y, Zhou G, Wu DS, Lee HR, Fan S, Cui Y. Nanoporous Polyethylene Microfibres for Large-scale Radiative Cooling Fabric. *Nat. Sustain.* **2018**, *1* (2), 105-112.

[19] Hu R, Wang N, Hou L, Liu J, Cui Z, Zhang C, Zhao Y. Bilayer Nanoporous Polyethylene Membrane with Anisotropic Wettability for Rapid Water Transportation/Evaporation and Radiative Cooling. *ACS Appl Mater Interfaces* **2022**, *14* (7), 9833-9843.

[20] Song Y-N, Lei M-Q, Deng L-F, Lei J, Li Z-M. Hybrid Metamaterial Textiles for Passive Personal Cooling Indoors and Outdoors. *ACS Appl. Polym. Mater.* **2020**, *2* (11), 4379-4386.

[21] Shi M, Shen M, Guo X, Jin X, Cao Y, Yang Y, Wang W, Wang J. Ti3C2Tx

MXene-Decorated Nanoporous Polyethylene Textile for Passive and Active Personal Precision Heating. *ACS Nano* **2021**, 11396-11405.

[22] Hsu PC, Liu X, Liu C, Xie X, Lee HR, Welch AJ, Zhao T, Cui Y. Personal Thermal Management by Metallic Nanowire-coated Textile. *Nano Lett* **2015**, *15* (1), 365-371.